

Dynamic Tensor Clustering

Will Wei Sun and Lexin Li

University of Miami and University of California at Berkeley

Abstract

Dynamic tensor data are becoming prevalent in numerous applications. Existing tensor clustering methods either fail to account for the dynamic nature of the data, or are inapplicable to a general-order tensor. Also there is often a gap between statistical guarantee and computational efficiency for existing tensor clustering solutions. In this article, we aim to bridge this gap by proposing a new dynamic tensor clustering method, which takes into account both sparsity and fusion structures, and enjoys strong statistical guarantees as well as high computational efficiency. Our proposal is based upon a new structured tensor factorization that encourages both sparsity and smoothness in parameters along the specified tensor modes. Computationally, we develop a highly efficient optimization algorithm that benefits from substantial dimension reduction. In theory, we first establish a non-asymptotic error bound for the estimator from the structured tensor factorization. Built upon this error bound, we then derive the rate of convergence of the estimated cluster centers, and show that the estimated clusters recover the true cluster structures with a high probability. Moreover, our proposed method can be naturally extended to co-clustering of multiple modes of the tensor data. The efficacy of our approach is illustrated via simulations and a brain dynamic functional connectivity analysis from an Autism spectrum disorder study.

Key Words: Cluster analysis; Multidimensional array; Non-convex optimization; Tensor decomposition; Variable selection.

¹Will Wei Sun is Assistant Professor, Department of Management Science, University of Miami School of Business Administration, Miami, FL 33146. Email: wsun@bus.miami.edu. Lexin Li is Associate Professor, Division of Biostatistics, University of California, Berkeley, Berkeley, CA 94720-3370. Email: lexinli@berkeley.edu.

1 Introduction

Data in the form of multidimensional array, or tensor, are now frequently arising in a diverse range of scientific and business applications (Zhu et al., 2007; Liu et al., 2013; Zhou et al., 2013; Ding and Cook, 2015). Particularly, for a large class of tensor data, time is one of the tensor modes, and this class is often termed as *dynamic tensor*. Examples of dynamic tensor data are becoming ubiquitous and its analysis are receiving increasing attention. For instance, in online advertising, Bruce et al. (2016) studied consumer engagement on advertisements over time to capture the temporal dynamics of users behavior. The resulting data is a three-mode tensor of user by advertisement by time. In molecular biology, Seigal et al. (2016) studied time-course measurements of the activation levels of multiple pathways from genetically diverse breast cancer cell lines after exposure to numerous growth factors with different dose. The data is a five-mode tensor of cell line by growth factor by pathway by dose by time. In neurogenomics, Liu et al. (2017) modeled spatial temporal patterns of gene expression during brain development, and the data is a three-mode tensor of gene by brain region by time. In Section 6, we illustrate our method on a brain dynamic connectivity analysis, where the goal is to understand interaction of distinct brain regions and their dynamic pattern over time. One form of the data in this context is a three-mode tensor of region by region by time.

Clustering has proven to be a useful tool to reveal important underlying data structures (Yuan and Kendzierski, 2006; Ma and Zhong, 2008; Shen et al., 2012a; Wang et al., 2013). Directly applying a clustering algorithm to the vectorized tensor data is a simple solution, but it often suffers from poor clustering accuracy, and incurs heavy and sometimes intractable computation. There have been a number of proposals for clustering of tensor data, or the two-mode special case, matrix data. One class of such methods focused on biclustering that simultaneously group rows (observations) and columns (features) of the data matrix (Huang et al., 2009; Lee et al., 2010; Chi and Lange, 2015; Chi and Allen, 2017). The proposed solutions were based on sparse singular value decomposition, or a reformulation of biclustering as a penalized regression with some convex penalties. However, the dynamic property remained largely untapped in those solutions. The second class of approaches directly targeted biclustering of time-varying matrix data (Hocking et al., 2011; Ji et al., 2012; Li et al., 2015). Nevertheless, those solutions were designed specifically for matrix-valued data. Extension to a general-order tensor is far from trivial. The third class tackled clustering of tensor data through some forms of ℓ_1 penalization (Cao et al., 2013; Wu et al., 2016).

But none of those approaches incorporated the dynamic information in the data and would inevitably lead to accuracy loss in clustering. Moreover, there is no statistical guarantee provided in the performance of these tensor clustering algorithms. *Tensor decomposition* is a crucial component in handling tensor-valued data, and is to play a central role in our proposed tensor clustering solution as well. There have been a number of recent proposals of convex relaxation of tensor decomposition through various norms (Romera-Paredes and Pontil, 2013; Yuan and Zhang, 2016a,b; Zhang, 2016). However, all those methods focused on low-rank tensor recovery, and none incorporated any sparsity or fusion structure in the decomposition. Recently, Sun et al. (2016) proposed a low-rank decomposition with a truncation operator for hard thresholding. Although sparsity was considered, they did not consider fusion structure for a dynamic tensor. Ignoring this structure, as we show later, would induce large estimation error in both tensor decomposition and subsequent clustering. In summary, there exists no clustering solution with statistical guarantees that handles a general-order dynamic tensor and incorporates both sparsity and fusion structures.

In this article, we aim to bridge this gap by proposing a dynamic tensor clustering method, which takes into account both sparsity and fusion structures, and enjoys strong statistical guarantee as well as high computational efficiency. Our proposal makes multiple contributions to the clustering literature. First, our clustering method is built upon a newly proposed structured tensor factorization approach, which encourages both sparsity and smoothness in the decomposed components, and in turn captures the dynamic nature of tensor data. We show how structured tensor factorization can be used to infer the clustering structure. Interestingly, we find that tensor Gaussian mixture model can be viewed as a special case of our clustering method. Second, our proposal is computationally efficient. This is partly achieved by substantial dimension reduction resulting from the imposed structure; in the illustrative example in Section 6, the number of free parameters was reduced from about two millions to one thousand. Our optimization algorithm can be decomposed as an unconstrained tensor decomposition step followed by a constrained optimization step. We show that, the overall computational complexity of our constrained solution is comparable to that of the unconstrained one. Third, and probably most importantly, we establish rigorous theoretical guarantees for our proposed dynamic tensor clustering solution. Specifically, we first establish a non-asymptotic error bound for the estimator from the proposed structured tensor factorization. Based on this error bound, we then obtain the rate of convergence of the estimated cluster centers from our dynamic tensor clustering solution, and prove

that the estimated clusters recover the true cluster structures with a high probability. It is also noteworthy that we allow the number of clusters to grow with the sample size. Such consistency results are new in the tensor clustering literature. From a technical perspective, the fusion structure we consider introduces some additional challenges in the theoretical analysis, since the resulting truncated fusion operator is non-convex and the observed tensor is usually noisy with an unknown error distribution. To address such challenges, we develop a set of non-asymptotic techniques to carefully evaluate the estimation error in each iteration of our alternating updating algorithm. We also utilize a series of large deviation bounds to show that our estimation error replies on the error term only through its sparse spectral norm, which largely relieves uncertainty from the unknown error distribution. Last but not least, although our algorithm mostly focuses on clustering along a single mode of tensor data, the same approach can be easily applied to co-clustering along multiple tensor modes. This is different from classical clustering methods, where an extension from clustering to bi-clustering generally requires different optimization formulations (see, e.g., [Chi and Allen, 2017](#)). In contrast, our clustering method naturally incorporates single and multi-mode clustering without requiring any additional modification.

The rest of the article is organized as follows. Section 2 introduces the proposed dynamic tensor clustering method, and Section 3 presents its solution through structured tensor factorization. Section 4 establishes the estimation error bound of the structured tensor factorization, then the consistency properties of dynamic tensor clustering. Section 5 presents the simulations, and Section 6 illustrates our method with a brain dynamic functional connectivity analysis. The appendix collects all technical proofs.

2 Model

2.1 Clustering via tensor factorization

Given N copies of m -way tensors, $\mathcal{X}_1, \dots, \mathcal{X}_N \in \mathbb{R}^{d_1 \times \dots \times d_m}$, our goal is to uncover the underlying cluster structures of these N samples. That is, we seek the true cluster assignment,

$$\underbrace{(1, \dots, 1)}_{l \text{ samples}}, \underbrace{(2, \dots, 2)}_{l \text{ samples}}, \dots, \underbrace{(K, \dots, K)}_{l \text{ samples}},$$

where K is the number of clusters and $l = N/K$. Here, for ease of presentation, we assume there are an equal number of l samples in each cluster.

To cluster those tensor samples, we first stack them into a $(m + 1)$ -way tensor, $\mathcal{T} \in \mathbb{R}^{d_1 \times \dots \times d_m \times N}$. We comment that, in principle, one can cluster along any single or multiple modes of \mathcal{T} . Without loss of generality, we focus our discussion on clustering along the last mode of \mathcal{T} , and only briefly comment on the scenario that clusters along multiple modes. This formulation covers a variety of scenarios encountered in our illustrative example of brain dynamic connectivity analysis. For instance, in one scenario, $\mathcal{T} \in \mathbb{R}^{p \times p \times t \times n}$, $N = n$, and the goal is to cluster n individuals, each with a $p \times p \times t$ tensor that represents the brain connectivity pattern among p brain regions over t sliding time windows. In another scenario, $\mathcal{T} \in \mathbb{R}^{p \times p \times t}$, $N = t$, and the goal is to cluster t sliding windows for a single subject. In the third scenario, $\mathcal{T} \in \mathbb{R}^{p \times p \times n_g \times t}$, $N = t$, where n_g is the number of subjects in group g , and the goal becomes clustering t moving windows for all subjects in that group.

Our key idea is to consider a structured decomposition of \mathcal{T} , then apply a usual clustering algorithm, e.g., K -means, to the matrix from the decomposition that corresponds to the last mode to obtain the cluster assignment. Specifically, we assume that the tensor \mathcal{T} is observed with noise; i.e.,

$$\mathcal{T} = \mathcal{T}^* + \mathcal{E}, \quad (1)$$

where \mathcal{E} is an error tensor, and \mathcal{T}^* is the true tensor with a rank- R CANDECOMP/PARAFAC (CP) decomposition structure (Kolda and Bader, 2009),

$$\mathcal{T}^* = \sum_{r=1}^R w_r^* \boldsymbol{\beta}_{1,r}^* \circ \dots \circ \boldsymbol{\beta}_{m+1,r}^*, \quad (2)$$

where $\boldsymbol{\beta}_{j,r}^* \in \mathbb{R}^{d_j}$, $\|\boldsymbol{\beta}_{j,r}^*\|_2 = 1$, and $w_r^* > 0$ for any $j = 1, \dots, m + 1$, $r = 1, \dots, R$. Here $\|\cdot\|_2$ denotes the vector ℓ_2 norm and \circ refers to the vector outer product. For ease of notation, we define $d_{m+1} := N$. Given the structure in (2), it is straightforward to see that, the cluster structure of samples along the last mode of the tensor \mathcal{T} is fully determined by the matrix that stacks the decomposition components, $\boldsymbol{\beta}_{m+1,1}^*, \dots, \boldsymbol{\beta}_{m+1,R}^*$. We denote this matrix as \mathbf{B}_{m+1} , which can be written as

$$\mathbf{B}_{m+1} := (\boldsymbol{\beta}_{m+1,1}^*, \dots, \boldsymbol{\beta}_{m+1,R}^*) \in \mathbb{R}^{N \times R} = \left(\underbrace{\boldsymbol{\mu}_1^{*\top}, \dots, \boldsymbol{\mu}_1^{*\top}}_{l \text{ samples}}, \dots, \underbrace{\boldsymbol{\mu}_K^{*\top}, \dots, \boldsymbol{\mu}_K^{*\top}}_{l \text{ samples}} \right)^\top,$$

where $\boldsymbol{\mu}_k^* := (\mu_{k,1}^*, \dots, \mu_{k,R}^*) \in \mathbb{R}^R$, $k = 1, \dots, K$, indicates the cluster assignment. Figure 1 shows a schematic illustration of our tensor clustering proposal. We comment that, if the

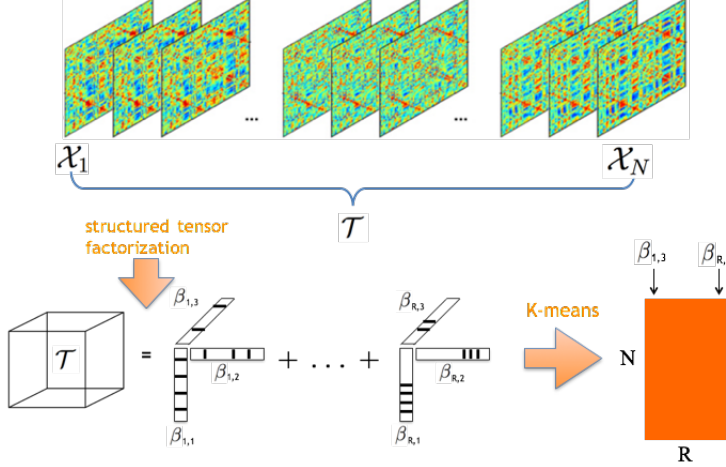


Figure 1: A schematic illustration of the proposed tensor clustering method. It stacks multiple tensor samples to a higher-order tensor, carries out structured tensor factorization, then applies a classical clustering algorithm, e.g, K -means, to the data matrix from the decomposition that corresponds to the last mode of the stacked tensor.

goal is to cluster along more than one tensor mode, one only needs to apply a clustering algorithm to the matrix formed by each of those modes separately.

Accordingly, the true cluster means of the tensor samples $\mathcal{X}_1, \dots, \mathcal{X}_N$ can be written as,

$$\mathcal{M}_1 := \underbrace{\sum_{r=1}^R w_r^* \beta_{1,r}^* \circ \dots \circ \beta_{m,r}^* \mu_{1,r}^*}_{\text{cluster center 1}}, \dots, \mathcal{M}_K := \underbrace{\sum_{r=1}^R w_r^* \beta_{1,r}^* \circ \dots \circ \beta_{m,r}^* \mu_{K,r}^*}_{\text{cluster center K}}. \quad (3)$$

The structure in (3) reveals the key underlying assumption of our tensor clustering solution. That is, we assume each cluster mean is a linear combination of the outer product of R rank-1 basis tensors, and all the cluster means share the same R basis tensors. We recognize that this assumption introduces an additional constraint. However, it leads to substantial dimension reduction, which in turn enables efficient estimation and inference in subsequent analysis. As we will show in Section 2.3, the tensor Gaussian mixture model can be viewed as a special case of our clustering structure. Moreover, as our numerical study has found, this imposed structure provides a reasonable approximation in real data applications.

As a comparison, we consider the alternative solution that applies clustering directly on the vectorized version of tensor data. It does not require (3), and the corresponding number of free parameters is in the order of $K \prod_j d_j$. In the example in Section 6, $d_1 = d_2 = 116, d_3 = 80, K = 2$, and that amounts to 2,152,960 parameters. Imposing (3),

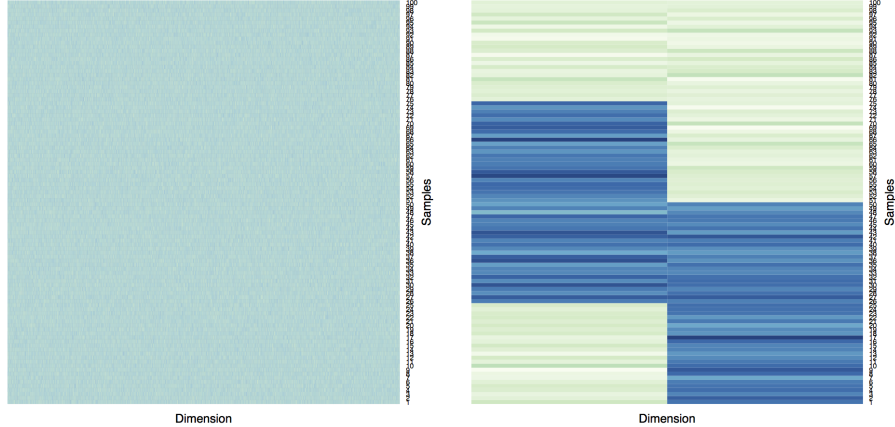


Figure 2: Heatmap of the vectorized data, with dimension 100×8000 , is shown in the left panel, and heatmap of the reduced data from our tensor factorization, with dimension 100×2 , is shown on the right. The true cluster structure can be fully recovered by any reasonable clustering method based on the reduced data, but not based on the vectorized data.

however, would reduce the number of free parameters to $R(\sum_j d_j + K + 1)$; again, for the aforementioned example, $R = 5$ and that amounts to 1,175 parameters. Such a substantial reduction in dimensionality is crucial for both computation and inference in tensor data analysis. Moreover, we use a simple simulation example to demonstrate that, our clustering method, which assumes (3) and thus exploits the underlying structure of the tensor data, can not only reduce the dimensionality and the computational cost, but also improve the clustering accuracy. Specifically, we follow the example in Section 5.2 to generate $N = 100$ tensor samples of dimension $d_1 = d_2 = d_3 = 20$ from 4 clusters, with samples 1 to 25, 26 to 50, 51 to 75, 76 to 100 belonging to clusters 1 to 4, respectively. Figure 2 shows the heatmap of the vectorized data (left panel), which is of dimension 100×8000 , and the heatmap of the data with reduced rank $R = 2$ (right panel), which is of dimension 100×2 . It is clearly seen from this plot that, our clustering method based on the reduced data under the structure (3) is able to fully recover the four underlying clusters, while the clustering method based on the vectorized data cannot.

2.2 Sparsity and fusion structures

Motivated from the brain dynamic functional connectivity analysis, in addition to the CP low-rank structure (2), we also impose sparsity and smoothness fusion structures in tensor decomposition to capture the sparsity and dynamic properties of the tensor samples.

Specifically, we impose the following structures in the parameter space,

$$\begin{aligned}\mathcal{S}(d, s_0) &:= \left\{ \boldsymbol{\beta} \in \mathbb{R}^d \mid \sum_{j=1}^d 1_{\{\beta_j \neq 0\}} \leq s_0 \right\}, \\ \mathcal{F}(d, f_0) &:= \left\{ \boldsymbol{\beta} \in \mathbb{R}^d \mid \sum_{j=2}^d |\beta_j - \beta_{j-1}| \leq f_0 \right\} = \left\{ \boldsymbol{\beta} \in \mathbb{R}^d \mid \|\mathbf{D}\boldsymbol{\beta}\|_1 \leq f_0 \right\},\end{aligned}$$

where $\boldsymbol{\beta} = (\beta_1, \dots, \beta_d)^\top$, $\|\cdot\|_1$ denotes the vector ℓ_1 norm, and

$$\mathbf{D} = \begin{pmatrix} -1 & 1 & 0 \cdots 0 & 0 \\ 0 & -1 & 1 \cdots 0 & 0 \\ \vdots & & & \\ 0 & 0 & 0 \cdots -1 & 1 \end{pmatrix} \in \mathbb{R}^{(d-1) \times d}.$$

Combining these two structures with the CP decomposition of \mathcal{T}^* in (2), we consider

$$\boldsymbol{\beta}_{j,r}^* \in \mathcal{S}(d_j, s_{0,j}) \cap \mathcal{F}(d_j, f_{0,j}), \text{ for any } j = 1, \dots, m+1, r = 1, \dots, R.$$

Here for simplicity, we assume the maximum of the sparsity parameter $s_{0,j}$ and the fusion parameter $f_{0,j}$ are the same across different rank $r = 1, \dots, R$, and we denote $s_0 := \max_j s_{0,j}$ and $f_0 := \max_j f_{0,j}$. This can be easily extended to a more general case where these parameters vary with r . To encourage such sparse and fused components, we propose to solve the following penalized optimization problem,

$$\begin{aligned}\min_{w_r, \boldsymbol{\beta}_{1,r}, \dots, \boldsymbol{\beta}_{m+1,r}} & \left\| \mathcal{T} - \sum_{r=1}^R w_r \boldsymbol{\beta}_{1,r} \circ \dots \circ \boldsymbol{\beta}_{m+1,r} \right\|_F^2 + \lambda \sum_{j=1}^{m+1} \sum_{r=1}^R \|\mathbf{D}\boldsymbol{\beta}_{j,r}\|_1, \\ \text{s.t. } & \|\boldsymbol{\beta}_{j,r}\|_2 = 1 \text{ and } \|\boldsymbol{\beta}_{j,r}\|_0 \leq s_j, \quad j = 1, \dots, m+1, r = 1, \dots, R,\end{aligned}\tag{4}$$

for some cardinality parameters s_1, \dots, s_{m+1} . Here $\|\cdot\|_0$ denotes the vector ℓ_0 norm, i.e., the number of nonzero entries, and $\|\cdot\|_F$ denotes the tensor Frobenius norm, which is defined as $\|\mathcal{A}\|_F := \sqrt{\sum_{i_1, \dots, i_m} \mathcal{A}_{i_1, \dots, i_m}^2}$ for a tensor $\mathcal{A} \in \mathbb{R}^{d_1 \times \dots \times d_m}$. This optimization formulation encourages sparsity in the individual components via a direct ℓ_0 constraint. Meanwhile, it encourages smoothness in the components via a fused lasso penalty. We note that, our optimization problem (4) is related to a recently proposed tensor decomposition method with generalized lasso penalties in [Madrid-Padilla and Scott \(2016\)](#). However, the two proposals differ in several ways. First, we use the ℓ_0 truncation to achieve sparsity, whereas they used the lasso penalty. It is known that former yields an unbiased estimator, while the latter leads

to a biased one in high-dimensional estimation (Shen et al., 2012b; Zhu et al., 2014). Second, our rate of convergence of the parameter estimators are established under a general error tensor, whereas theirs required the error tensor to be Gaussian.

2.3 A special case: tensor Gaussian mixture model

In model (1), no distributional assumption is imposed on the error tensor \mathcal{E} . In this section, we show that, if one further assumes that \mathcal{E} is a standard Gaussian tensor, then our method reduces to a tensor version of Gaussian mixture model.

An m -way tensor $\mathcal{X} \in \mathbb{R}^{d_1 \times d_2 \times \dots \times d_m}$ is said to follow a tensor normal distribution (Kolda and Bader, 2009) with mean \mathcal{M} and covariance matrices, $\Sigma_1, \dots, \Sigma_m$, denoted as $\mathcal{X} \sim \text{TN}(\mathcal{M}; \Sigma_1, \dots, \Sigma_m)$, if and only if $\text{vec}(\mathcal{X}) \sim N(\text{vec}(\mathcal{M}), \otimes_{j=1}^m \Sigma_j)$, where $\text{vec}(\mathcal{M}) \in \mathbb{R}^{\prod_j d_j}$, vec denotes the tensor vectorization, and \otimes denotes the matrix Kronecker product. Following the usual definition of Gaussian mixture model, we say \mathcal{X} is drawn from a tensor Gaussian mixture model, if its density function is of the form,

$$f(\mathcal{X}) = \sum_{k=1}^K \pi_k \phi_k(\mathcal{M}_k; \Sigma_{k,1}, \dots, \Sigma_{k,m}),$$

where π_k is the mixture weight, and $\phi_k(\mathcal{M}_k; \Sigma_{k,1}, \dots, \Sigma_{k,m})$ is the probability density function of a tensor Gaussian distribution $\text{TN}(\mathcal{M}_k; \Sigma_{k,1}, \dots, \Sigma_{k,m})$. We next consider two special cases of our general tensor clustering model (1).

First, when the error tensor \mathcal{E} in (1) is a standard Gaussian tensor, then our clustering model is equivalent to assuming the tensor-valued samples $\mathcal{X}_i, i = 1, \dots, N$, follow the above tensor Gaussian mixture model. That is,

$$\begin{aligned} \mathcal{X}_1, \dots, \mathcal{X}_l &\sim TN(\mathcal{M}_1^*; \mathbf{I}_{d_1}, \dots, \mathbf{I}_{d_m}), \\ &\dots \\ \mathcal{X}_{N-l}, \dots, \mathcal{X}_N &\sim TN(\mathcal{M}_K^*; \mathbf{I}_{d_1}, \dots, \mathbf{I}_{d_m}), \end{aligned}$$

where \mathbf{I}_d is a $d \times d$ identity matrix. As such, the tensor samples $\mathcal{X}_1, \dots, \mathcal{X}_N$ are drawn from a tensor Gaussian mixture model with the k th cluster center \mathcal{M}_k^* and the k th prior probability $\pi_k = 1/K$, for $k = 1, \dots, K$.

Second, when the error tensor \mathcal{E} in (1) is a general Gaussian tensor, then our model is

equivalent to assuming the samples follow

$$\begin{aligned}\mathcal{X}_1, \dots, \mathcal{X}_l &\sim TN(\mathcal{M}_1^*; \Sigma_{1,1}, \dots, \Sigma_{1,m}), \\ &\dots \\ \mathcal{X}_{N-l}, \dots, \mathcal{X}_N &\sim TN(\mathcal{M}_K^*; \Sigma_{K,1}, \dots, \Sigma_{K,m}),\end{aligned}$$

where $\Sigma_{k,j}$ is a general covariance matrix, $k = 1, \dots, K, j = 1, \dots, m$. In our proposed clustering solution, we have chosen not to estimate those covariances matrices. This greatly simplifies both the computation and theoretical analysis. However, the methodology we develop can be extended to incorporate general covariances $\Sigma_{k,j}$ in a straightforward fashion. The sample estimators of $\Sigma_{k,j}$ can be obtained using, e.g., [Leng and Tang \(2012\)](#); [Zhu et al. \(2014\)](#); [Xu et al. \(2017\)](#), then plugged into our tensor clustering algorithm. In the interest of space, we do not pursue this line but leave it as potential future research.

3 Estimation

3.1 Optimization algorithm

We first introduce some operators for achieving the sparsity and fusion structures of a given dense vector. We then present our optimization algorithm.

The first operator is a truncation operator to obtain the sparse structure. For a vector $\mathbf{v} \in \mathbb{R}^d$ and a scalar $\tau \leq d$, we define $\text{Truncate}(\mathbf{v}, \tau)$ as

$$[\text{Truncate}(\mathbf{v}, \tau)]_j = \begin{cases} v_j & \text{if } j \in \text{supp}(\mathbf{v}, \tau) \\ 0, & \text{otherwise} \end{cases},$$

where $\text{supp}(\mathbf{v}, \tau)$ refers to the set of indices of \mathbf{v} corresponding to its largest τ absolute values. The second is a fusion operator. For a vector $\mathbf{v} \in \mathbb{R}^d$ and a fusion parameter $\lambda > 0$, the fused vector $\text{Fuse}(\mathbf{v}, \lambda)$ is obtained via the fused lasso ([Tibshirani et al., 2005](#)); i.e.,

$$\text{Fuse}(\mathbf{v}, \lambda) := \arg \min_{\mathbf{u} \in \mathbb{R}^d} \left\{ \sum_{i=1}^d (u_i - v_i)^2 + \lambda \|\mathbf{D}\mathbf{u}\|_1 \right\}.$$

An efficient ADMM-based algorithm for this fused lasso has been developed in [Zhu \(2017\)](#). The third operator is a combination of the truncation and fusion operators. For $\mathbf{v} \in \mathbb{R}^d$ and parameters τ, λ , we define $\text{Truncatefuse}(\mathbf{v}, \tau, \lambda)$ as

$$\text{Truncatefuse}(\mathbf{v}, \tau, \lambda) = \text{Truncate}\left(\text{Fuse}(\mathbf{v}, \lambda), \tau\right).$$

Algorithm 1 Structured tensor factorization for optimization of (4).

- 1: **Input:** tensor \mathcal{T} , rank R , cardinalities (s_1, \dots, s_{m+1}) , fusion parameters $(\lambda_1, \dots, \lambda_{m+1})$.
- 2: For $r = 1$ to R
- 3: Initialize unit-norm vectors $\widehat{\beta}_{j,r}^{(0)}$ randomly for $j = 1, \dots, m+1$.
- 4: Repeat
- 5: For $j = 1$ to $m+1$
- 6: Update $\widehat{\beta}_{j,r}^{(\kappa+1)}$ as

$$\widetilde{\beta}_{j,r}^{(\kappa+1)} = \text{Norm}\left(\widehat{\beta}_{1,r}^{(\kappa)} \times_2 \dots \widehat{\beta}_{j-1,r}^{(\kappa)} \times_j \mathcal{T} \times_{j+1} \widehat{\beta}_{j+1,r}^{(\kappa)} \times_{j+2} \dots \times_{m+1} \widehat{\beta}_{m+1,r}^{(\kappa)}\right), \quad (5)$$

$$\check{\beta}_{j,r}^{(\kappa+1)} = \text{Truncatefuse}\left(\widetilde{\beta}_{j,r}^{(\kappa+1)}, s_j, \lambda_j\right), \quad (6)$$

$$\widehat{\beta}_{j,r}^{(\kappa+1)} = \text{Norm}\left(\check{\beta}_{j,r}^{(\kappa+1)}\right). \quad (7)$$

- 7: End For
- 8: Until the termination condition is met.
- 9: Compute $\widehat{w}_r = \mathcal{T} \times_1 \widehat{\beta}_{1,r}^{(\kappa_{max})} \times_2 \dots \times_m \widehat{\beta}_{m+1,r}^{(\kappa_{max})}$, where κ_{max} is the terminated iteration.
- 10: Update the tensor $\mathcal{T} = \mathcal{T} - \widehat{w}_r \widehat{\beta}_{1,r}^{(\kappa_{max})} \circ \dots \circ \widehat{\beta}_{m+1,r}^{(\kappa_{max})}$.
- 11: End For
- 12: **Output:** \widehat{w}_r and $\widehat{\beta}_{j,r}^{(\kappa_{max})}$ for $j = 1, \dots, m+1$ and $r = 1, \dots, R$.

Lastly, we denote $\text{Norm}(\mathbf{v}) = \mathbf{v}/\|\mathbf{v}\|$ as the normalization operator on a vector \mathbf{v} .

We propose a structured tensor factorization procedure, and summarizes it in Algorithm 1. It consists of three major steps. Specifically, the step in (5) essentially obtains an unconstrained tensor decomposition, and is done through the classical tensor power method (Anandkumar et al., 2014). Here, for a tensor $\mathcal{A} \in \mathbb{R}^{d_1 \times \dots \times d_m}$ and a set of vectors $\mathbf{a}_j \in \mathbb{R}^{d_j}, j = 1, \dots, m$, the multilinear combination of the tensor entries is defined as $\mathcal{A} \times_1 \mathbf{a}_1 \times_2 \dots \times_m \mathbf{a}_m := \sum_{i_1 \in [d_1]} \dots \sum_{i_m \in [d_m]} a_{i_1} \dots a_{i_m} \mathcal{A}_{i_1, \dots, i_m} \in \mathbb{R}$. It is then followed by our new Truncatefuse step in (6) to generate a sparse and fused component. Finally, the step in (7) normalizes the component to ensure the unit-norm. These three steps form a full update cycle of one decomposition component. The algorithm then updates all components in an alternating fashion, until some termination condition is satisfied. In our implementation, the algorithm terminates if the total number of iterations exceeds 20, or $\sum_{j=1}^{m+1} \|\widehat{\beta}_{j,r}^{(\kappa+1)} - \widehat{\beta}_{j,r}^{(\kappa)}\|_2^2 \leq 10^{-4}$.

In terms of computational complexity, we note that, the complexity of operation in (5) is $O(\prod_{j=1}^{m+1} d_j)$, while the complexity in (6) consists of $O(d_j \log d_j)$ for the truncation operation and $O(d_j^3)$ for the fusion operation (Tibshirani and Taylor, 2011). Therefore, the total complexity of Algorithm 1 is $O(R\kappa_{max} \max\{m \prod_{j=1}^{m+1} d_j, \sum_{j=1}^{m+1} d_j^3\})$. It is interesting

Algorithm 2 Dynamic tensor clustering procedure

- 1: **Input:** Tensor samples $\mathcal{X}_1, \dots, \mathcal{X}_N \in \mathbb{R}^{d_1 \times \dots \times d_m}$, number of clusters K , cardinalities (s_1, \dots, s_{m+1}) , fusion parameters $(\lambda_1, \dots, \lambda_{m+1})$, rank R .
- 2: **Step 1:** Stack tensor samples into a higher-order tensor $\mathcal{T} \in \mathbb{R}^{d_1 \times \dots \times d_m \times N}$, where the i -th slice in the last mode is \mathcal{X}_i .
- 3: **Step 2:** Apply Algorithm 1 to \mathcal{T} with rank R , cardinalities (s_1, \dots, s_{m+1}) , and fusion parameters $(\lambda_1, \dots, \lambda_{m+1})$ to obtain $\widehat{\mathbf{B}}_{m+1} = (\widehat{\boldsymbol{\beta}}_{m+1,1}^{(\kappa_{max})}, \dots, \widehat{\boldsymbol{\beta}}_{m+1,R}^{(\kappa_{max})}) \in \mathbb{R}^{N \times R}$.
- 4: **Step 3:** Apply the K -means clustering to $\widehat{\mathbf{B}}_{m+1}$ by treating each row as a sample.
- 5: **Output:** Cluster assignments $\mathcal{A}_1, \dots, \mathcal{A}_K$ from **Step 3**.

to note that, when the tensor order $m > 2$ and the dimension d_j along each tensor mode is of a similar value, the complexity of the sparsity and fusion operation in (6) is to be dominated by that in (5). Consequently, our addition of sparsity and fusion structures does not substantially increase the overall complexity of the tensor decomposition.

Based upon the structured tensor factorization, we next summarize in Algorithm 2 our proposed dynamic tensor clustering procedure illustrated in Figure 1. It is noted that Step 2 of Algorithm 2 utilizes the structured tensor factorization to obtain a reduced data $\widehat{\mathbf{B}}_{m+1}$, whose columns consist of all information of the original samples that are relevant to clustering. This avoids the curse of dimensionality through substantial dimension reduction. We also note that Step 2 provides a reduced data along each mode of the original tensor, and hence it is straightforward to achieve co-clustering of any single or multiple tensor modes. This is different from the classical clustering methods, where extension from clustering to bi-clustering generally requires different optimization formulations (see, e.g., [Chi and Allen, 2017](#)).

3.2 Application example: brain dynamic connectivity analysis

Our proposed dynamic tensor clustering approach applies to many different applications involving dynamic tensor. Here we consider one specific application, brain dynamic connectivity analysis. Brain functional connectivity describes interaction and synchronization of distinct brain regions, and is characterized by a network, with nodes representing regions, and links measuring pairwise dependency between regions. This dependency is frequently quantified by Pearson correlation coefficient, and the resulting connectivity network is a region by region correlation matrix ([Fornito et al., 2013](#)). Traditionally, it is assumed that connectivity networks do not change over time when a subject is resting during the scan. However, there is growing evidence suggesting the contrary that networks are not static but

dynamic over the time course of scan (Aston and Kirch, 2012; Hutchison et al., 2013). To capture such dynamic changes, a common practice is to introduce sliding and overlapping time windows, compute the correlation network within each window, then apply a clustering method to identify distinct states of connectivity patterns over time (Allen et al., 2014).

There are several scenarios within this context, which share some similar characteristics. The first scenario is when we aim to cluster n individual subjects, each represented by a $p \times p \times t$ tensor that describes the brain connectivity pattern among p brain regions over t sliding and overlapping time windows. Here n denotes the sample size, p the number of brain regions, and t the total number of moving windows. In this case, $\mathcal{T} \in \mathbb{R}^{p \times p \times t \times n}$ and $N = n$. It is natural to encourage sparsity in the first two modes of \mathcal{T} , and thus to improve interpretability and identification of connectivities among important brain regions. Meanwhile, it is equally intuitive to encourage smoothness along the time mode of \mathcal{T} , since the connectivity patterns among the adjacent and overlapping time windows are indeed highly correlated and similar. Toward that end, we propose the following structured tensor factorization based clustering solution, by considering the minimization problem,

$$\begin{aligned} & \min_{w_r, \beta_{1,r}, \beta_{2,r}, \beta_{3,r}, \beta_{4,r}} \left\| \mathcal{T} - \sum_{r=1}^R w_r \beta_{1,r} \circ \beta_{2,r} \circ \beta_{3,r} \circ \beta_{4,r} \right\|_F^2 + \lambda \sum_{r=1}^R \|\mathbf{D}\beta_{3,r}\|_1. \\ & \text{s.t. } \|\beta_{j,r}\|_2 = 1, j = 1, \dots, 4, \beta_{1,r} = \beta_{2,r}, \text{ and } \|\beta_{1,r}\|_0 \leq s, r = 1, \dots, R, \end{aligned}$$

where s and λ are the cardinality and fusion parameters, respectively. This optimization problem can be solved via Algorithm 1. Given that the connectivity matrix is symmetric, i.e., \mathcal{T} is symmetric in its first two modes, we can easily incorporate such a symmetry constraint by setting $\widehat{\beta}_{2r}^{(t+1)} = \widehat{\beta}_{1r}^{(t+1)}$ in Algorithm 1.

Another scenario is to cluster t sliding windows for a single subject, so to examine if the connectivity pattern is dynamic or not over time. Here $\mathcal{T} \in \mathbb{R}^{p \times p \times t}$ and $N = t$. In this case, we consider the following minimization problem,

$$\begin{aligned} & \min_{w_r, \beta_{1,r}, \beta_{2,r}, \beta_{3,r}} \left\| \mathcal{T} - \sum_{r=1}^R w_r \beta_{1,r} \circ \beta_{2,r} \circ \beta_{3,r} \right\|_F^2 + \lambda \sum_{r=1}^R \|\mathbf{D}\beta_{3,r}\|_1. \\ & \text{s.t. } \|\beta_{j,r}\|_2 = 1, j = 1, \dots, 3, \beta_{1,r} = \beta_{2,r}, \text{ and } \|\beta_{1,r}\|_0 \leq s, r = 1, \dots, R. \end{aligned}$$

If one is to examine the dynamic connectivity pattern for n_g subjects simultaneously, then $\mathcal{T} \in \mathbb{R}^{p \times p \times n_g \times t}$. Both problems can be solved by dynamic tensor clustering in Algorithm 2.

3.3 Tuning

Our clustering algorithm involves a number of tuning parameters. To facilitate the computation, we propose a multi-step tuning procedure. We first choose the rank R , the sparsity parameters s_1, \dots, s_{m+1} , and the fusion parameters $\lambda_1, \dots, \lambda_{m+1}$ via

$$\text{BIC} := \log \left(\frac{\|\mathcal{T} - \sum_{r \in [R]} \hat{w}_r \hat{\beta}_{1,r} \circ \dots \circ \hat{\beta}_{m+1,r}\|_F^2}{\prod_{j=1}^{m+1} d_j} \right) + \frac{\sum_{j=1}^{m+1} \log d_j}{\prod_{j=1}^{m+1} d_j} \times p_e,$$

where p_e refers to the degrees of freedom. Such a BIC-type criterion has been widely used in model selection (Wang, 2015). For simplicity, it is not uncommon to set $s = s_1 = \dots = s_{m+1}$ and $\lambda = \lambda_1 = \dots = \lambda_{m+1}$. Here the degrees of freedom p_e can be estimated by the number of non-zero elements under a sparsity penalty, and by the number of unique elements under a fusion penalty. Accordingly, we define the degrees of freedom of an individual component $p_e(\beta)$ as the number of unique non-zero elements in a vector β , and estimate the total degrees of freedom via $p_e = \sum_{j=1}^{m+1} \sum_{r \in [R]} p_e(\hat{\beta}_{j,r})$. Finally, we employ a well established gap statistic (Tibshirani et al., 2001) to tune the number of clusters K . The gap statistic selects the best K as the minimal one such that $gap(k) \geq gap(k+1) - se(k+1)$, where $se(k+1)$ is the standard error corresponding to the $(k+1)$ th gap statistic. In the literature, stability-based methods (Wang, 2010; Wang and Fang, 2013) have also been proposed that can consistently select the number of clusters. We choose the gap statistic due to its computational simplicity, and leave the investigation of its selection consistency as future research.

4 Theory

4.1 Theory of structured tensor factorization

We begin with the derivation of the rate of convergence of the general structured tensor factorization estimator from Algorithm 1. Recall that we observe the tensor \mathcal{T} with noise as specified in (1). To quantify the noise level of the error tensor, we define the sparse spectral norm of $\mathcal{E} \in \mathbb{R}^{d_1 \times \dots \times d_{m+1}}$ as,

$$\eta(\mathcal{E}; s_1^*, \dots, s_{m+1}^*) := \sup_{\substack{\|\mathbf{u}_1\| = \dots = \|\mathbf{u}_{m+1}\| = 1 \\ \|\mathbf{u}_1\|_0 \leq s_1^*, \dots, \|\mathbf{u}_{m+1}\|_0 \leq s_{m+1}^*}} \left| \mathcal{E} \times_1 \mathbf{u}_1 \times_2 \dots \times_{m+1} \mathbf{u}_{m+1} \right|,$$

where $s_j^* \leq d_j$ for $j = 1, \dots, m+1$. This term quantifies the perturbation error in a sparse scenario. We then have the following general result.

Theorem 1. Consider the structure in (2) with $R = 1$. Assume the true decomposition components are sparse and smooth in that $\|\mathbf{D}\beta_j^*\|_1 \leq f_{0,j}$ and $\|\beta_j^*\|_0 \leq s_{0j}$ for $j = 1, \dots, m+1$. Define $M := \max_j \|[\mathbf{D}^\dagger]_j\|_2$, where \mathbf{D}^\dagger is the pseudoinverse of \mathbf{D} and $[\mathbf{D}^\dagger]_j$ refers to its j -th column. Assume the initialization satisfies $\|\widehat{\beta}_j^{(0)} - \beta_j^*\|_2 \leq \epsilon_0$, $j = 1, \dots, m$, with $\epsilon_0 < 1$. If $s_j \geq s_{0j}$, and the error tensor satisfies $\eta(\mathcal{E}; s_1, \dots, s_{m+1}) < w^*(1 - \epsilon_0^2)$, then $\widehat{\beta}_{m+1}^{(1)}$ of our algorithm with $\lambda_{m+1} \geq 2M\eta(\mathcal{E}; s_1, \dots, s_{m+1})/[w^*(1 - \epsilon_0^2) - \eta(\mathcal{E}; s_1, \dots, s_{m+1})]$ satisfies, with a high probability,

$$\|\widehat{\beta}_{m+1}^{(1)} - \beta_{m+1}^*\|_2^2 \leq \left[\frac{2\eta(\mathcal{E}; s_1, \dots, s_{m+1})}{w^*(1 - \epsilon_0^2) - \eta(\mathcal{E}; s_1, \dots, s_{m+1})} \right]^2 + \frac{8Mf_{0,m+1}\eta(\mathcal{E}; s_1, \dots, s_{m+1})}{w^*(1 - \epsilon_0^2) - \eta(\mathcal{E}; s_1, \dots, s_{m+1})}. \quad (8)$$

The proof of this theorem is given in the Appendix. We make a few remarks regarding both the conditions and the implication of this theorem. First, we recognize that $0 \leq \epsilon_0 \leq 1$, since the components are normalized to have a unit norm. Our condition on the initial error is very weak, by noting that we only require the initialization to be slightly better than a naive estimator whose entries are all zeros so to avoid $\epsilon_0 = 1$. As such, the proposed random initialization in our algorithm satisfies this condition with high probability. Second, when ϵ_0 is a constant strictly less than 1, we see a clear tradeoff between the signal level w^* and the error tensor \mathcal{E} according to the condition $\eta(\mathcal{E}; s_1, \dots, s_{m+1}) < w^*(1 - \epsilon_0^2)$. Third, the derived upper bound in (8) reveals an interesting interaction of the initial error ϵ_0 , the signal level w^* , and the error tensor \mathcal{E} . Apparently, the error bound can be reduced by lowering ϵ_0 or \mathcal{E} , or increasing w^* . For a fixed signal level w^* , more noisy samples, i.e., a larger \mathcal{E} , would require a more accurate initialization in order to obtain the same error bound. Moreover, this error bound is a monotonic function of the smoothness parameter $f_{0,m+1}$. In contrast to the non-smoothed tensor factorization with $f_{0,m+1} = d_{m+1}$, our structured tensor factorization is able to greatly reduce the error bound, since $f_{0,m+1}$ is usually much smaller than d_{m+1} in the dynamic scenario. Finally, for ease of presentation, we state our result under the rank $R = 1$ case. For the general rank- R case, additional incoherent assumptions on the decomposition components are required in order to ensure the correlation between the decomposed components from different ranks are not too large (Sun et al., 2016).

Based on the general rate derived in Theorem 1, the next result shows that Algorithm 1 generates a contracted estimator. It is thus guaranteed that the estimator converges to the truth as the number of iterations increases.

Corollary 1. *Assume the conditions in Theorem 1 hold. Furthermore, assume the error tensor satisfies*

$$\eta(\mathcal{E}; s_1, \dots, s_{m+1}) \leq \min \left\{ \frac{w^* \epsilon_0 (1 - \epsilon_0)}{9}, \frac{w^* \epsilon_0^2 (1 - \epsilon_0)}{32M f_{0,m+1} + 1} \right\}.$$

If $\|\widehat{\beta}_j^{(0)} - \beta_j^*\|_2 \leq \epsilon_0$, $j = 1, \dots, m$, then the update $\widehat{\beta}_{m+1}^{(1)}$ in our algorithm satisfies $\|\widehat{\beta}_{m+1}^{(1)} - \beta_{m+1}^*\|_2 \leq \epsilon_0/2$ with a high probability.

Corollary 1 implies that the ℓ_2 distance of the estimator to the truth from each iteration is at most half of the one from the previous iteration. Simple algebra implies that the estimator in the κ -th iteration of the algorithm satisfies $\|\widehat{\beta}_{m+1}^{(\kappa)} - \beta_{m+1}^*\|_2 \leq 2^{-\kappa} \epsilon_0$, which converges to zero as κ increases. Here the assumption on $\eta(\mathcal{E}; s_1, \dots, s_{m+1})$ is imposed to ensure that the contraction rate of the estimator is $1/2$, and it can be relaxed for a slower contraction rate.

It is also noteworthy that the above results do not require specification of the error tensor distribution. Next we derive the explicit form of the estimation error in Theorem 1 when \mathcal{E} is a Gaussian tensor.

Corollary 2. *Assume the conditions of Theorem 1, and assume $\mathcal{E} \in \mathbb{R}^{d_1 \times \dots \times d_{m+1}}$ is a Gaussian tensor. Then we have $\eta(\mathcal{E}; s_1, \dots, s_{m+1}) = C \sqrt{\prod_{j=1}^{m+1} s_j \sum_{j=1}^{m+1} \log(d_j)}$ for some constant C . In addition, if the signal strength satisfies $w^* \succ \sqrt{\prod_{j=1}^{m+1} s_j \sum_{j=1}^{m+1} \log(d_j)}$, we have the update $\widehat{\beta}_{m+1}^{(1)}$ in one iteration of our algorithm satisfies*

$$\|\widehat{\beta}_{m+1}^{(1)} - \beta_{m+1}^*\|_2^2 = \widetilde{O}_p \left(\max \left\{ \frac{\prod_{j=1}^{m+1} s_j}{w^{*2}}, \frac{f_{0,m+1} \sqrt{\prod_{j=1}^{m+1} s_j}}{w^*} \right\} \right),$$

where $a_n = \widetilde{O}_p(b_n)$ means $a_n = O_p(b_n)$ up to a logarithm term.

4.2 Theory of dynamic tensor clustering

Next we establish the consistency properties of our proposed dynamic tensor clustering solution under the tensor Gaussian mixture model. Again we consider the case when $R = 1$, while the result can be extended to a general rank case. Consider a collection of m -way tensor samples, $\mathcal{X}_1, \dots, \mathcal{X}_N \in \mathbb{R}^{d_1 \times d_2 \times \dots \times d_m}$, from a tensor Gaussian mixture model, with K rank-1 centers, $\mathcal{M}_1 := \mu_1^* w^* \beta_1^* \circ \dots \circ \beta_m^*, \dots, \mathcal{M}_K := \mu_K^* w^* \beta_1^* \circ \dots \circ \beta_m^*$, and equal prior

probability $\pi_k = 1/K$, for $k = 1, \dots, K$. As before, we assume an equal number of $l = N/K$ samples in each cluster. We denote the component from the last mode β_{m+1}^* as,

$$\beta_{m+1}^* = (\underbrace{\mu_1^*, \dots, \mu_1^*}_{l \text{ samples}}, \underbrace{\mu_2^*, \dots, \mu_2^*}_{l \text{ samples}}, \dots, \underbrace{\mu_K^*, \dots, \mu_K^*}_{l \text{ samples}}). \quad (9)$$

Define the true cluster assignment as $\mathcal{A}_1^* := \{1, \dots, l\}, \dots, \mathcal{A}_K^* := \{N - l, \dots, N\}$, and the estimated cluster assignment as $\hat{\mathcal{A}}_1, \dots, \hat{\mathcal{A}}_K$. Then we show that our proposed dynamic tensor clustering estimator is consistent, in that the estimated cluster centers from our dynamic tensor clustering converge to the truth consistently, and that the estimated clusters recover the true cluster structures with a high probability.

Theorem 2. *Assume $\|\beta_j^*\|_0 \leq s_{0,j}$ and $\|\mathbf{D}\beta_j^*\|_1 \leq f_{0,j}$ for $j = 1, \dots, m$. Assume β_{m+1}^* is of the form (9). Define $M := \max_j \|\mathbf{D}^\dagger\|_2$. Assume the initialization satisfies $\|\hat{\beta}_j - \beta_j^*\|_2 \leq \epsilon_0$, $j = 1, \dots, m$, with $\epsilon_0 < 1$. If $s_j \geq s_{0,j}$ for $j = 1, \dots, m$ and the signal strength satisfies $w^* \succ \sqrt{\prod_{j=1}^m s_j N^2 \log(\prod_{j=1}^m d_j N)/K}$, then the estimator $\hat{\beta}_{m+1}$ satisfies*

$$\|\hat{\beta}_{m+1} - \beta_{m+1}^*\|_2 = O_p\left(\frac{K}{\sqrt{N}}\right).$$

Moreover, if $\min_{i,j} |\mu_i^* - \mu_j^*| > C_1 K / \sqrt{N}$ for some constant C_1 , we have $\hat{\mathcal{A}}_k = \mathcal{A}_k^*$ for any $k = 1, \dots, K$, with a high probability.

Compared to Corollary 2 for the general structured tensor factorization, Theorem 2 requires a stronger condition on the signal strength w^* in order to ensure the estimation error of cluster centers converges to zero at a desirable rate. Given this rate and an additional condition on the minimal gap between clusters, we are able to ensure that the estimated clusters recover the true clusters with a high probability. It is also worth mentioning that our theory allows the number of clusters K to diverge polynomially with the sample size N , reflecting a typical big data scenario.

5 Simulations

5.1 Setup and evaluation

We consider two simulation experiments: clustering of two-dimensional matrix samples, and clustering of three-dimensional tensor samples. We assess the performance in two ways: the

accuracy of the recovered tensor decomposition components, and the accuracy of the cluster assignment. To evaluate the decomposition accuracy, we calculate the tensor decomposition error as the average of the mean vector estimation error and weight estimation error, i.e.,

$$\text{decomposition error} = \frac{1}{2} \left\{ \sum_{r=1}^R \sum_{j=1}^{m+1} \|\widehat{\boldsymbol{\beta}}_{r,j} - \boldsymbol{\beta}_{r,j}^*\|_2 + \frac{\|\widehat{w} - w^*\|_2}{\|w^*\|_2} \right\}.$$

When the estimated rank from tuning is not equal to the true rank, the estimation error is computed by either truncating the estimated rank to the true rank if the estimated one is larger, or filling with zeros if the estimated rank is smaller. To evaluate the clustering accuracy, we define the clustering error as the estimated distance between an estimated cluster assignment $\widehat{\psi}$ and the true assignment ψ of the sample data $\mathcal{X}_1, \dots, \mathcal{X}_N$, i.e.,

$$\text{clustering error} = \binom{N}{2}^{-1} \left| \{(i, j) : 1(\widehat{\psi}(\mathcal{X}_i) = \widehat{\psi}(\mathcal{X}_j)) \neq 1(\psi(\mathcal{X}_i) = \psi(\mathcal{X}_j)); i < j\} \right|,$$

where $|A|$ is the cardinality of the set A . This criterion has been commonly used in the clustering literature (Wang, 2010).

We compare our proposed method with some alternative solutions. For tensor decomposition, we compare our structured tensor factorization method with two alternative tensor decomposition solutions, the tensor truncated power method of Sun et al. (2016), and the generalized lasso penalized tensor decomposition method of Madrid-Padilla and Scott (2016). For clustering, our solution is to apply K -means to the last component from our structured tensor factorization. Therefore, we compare with the solutions of applying K -means to the component from the decomposition method of Sun et al. (2016) and Madrid-Padilla and Scott (2016), respectively, and to the vectorized tensor data without any tensor decomposition. The solution of clustering the vectorized data is often used in brain dynamic functional connectivity analysis (Allen et al., 2014).

5.2 Clustering of 2D matrix data

We simulate the matrix observations, $\mathcal{X}_i \in \mathbb{R}^{d_1 \times d_2}$, $i = 1, \dots, N$, based on the decomposition model in (2) with a true rank $R = 2$. The unnormalized components $\widetilde{\boldsymbol{\beta}}_{r,j}^*$ are generated as,

$$\begin{aligned} \widetilde{\boldsymbol{\beta}}_{11}^* &= \widetilde{\boldsymbol{\beta}}_{21}^* = (\mu, -\mu, 0.5\mu, -0.5\mu, 0, \dots, 0), \quad \widetilde{\boldsymbol{\beta}}_{31}^* = (\underbrace{\mu, \dots, \mu}_{\lfloor N/2 \rfloor}, \underbrace{-\mu, \dots, -\mu}_{\text{the rest}}); \\ \widetilde{\boldsymbol{\beta}}_{12}^* &= \widetilde{\boldsymbol{\beta}}_{22}^* = (0, 0, 0, 0, \mu, -\mu, 0.5\mu, -0.5\mu, 0, \dots, 0), \quad \widetilde{\boldsymbol{\beta}}_{32}^* = (\underbrace{-\mu, \dots, -\mu}_{\lfloor N/4 \rfloor}, \underbrace{\mu, \dots, \mu}_{\lfloor N/2 \rfloor}, \underbrace{-\mu, \dots, -\mu}_{\text{the rest}}). \end{aligned}$$

We then obtain the true components $\beta_{rj}^* = \text{Norm}(\tilde{\beta}_{rj}^*)$, and the corresponding norm is absorbed into the tensor weight w^* . We set $d_1 = d_2$ and vary $d_1 = \{20, 40\}$, the sample size $N = \{50, 100\}$, and the signal level $\mu = \{1, 1.2\}$. The components $\tilde{\beta}_{31}^*$ and $\tilde{\beta}_{32}^*$ determine the cluster structures of the matrix samples, resulting in four clusters, with $\mathcal{X}_1, \dots, \mathcal{X}_{\lfloor N/4 \rfloor} \in \mathcal{A}_1$, $\mathcal{X}_{\lfloor N/4 \rfloor + 1}, \dots, \mathcal{X}_{\lfloor N/2 \rfloor} \in \mathcal{A}_2$, $\mathcal{X}_{\lfloor N/2 \rfloor + 1}, \dots, \mathcal{X}_{\lfloor 3N/4 \rfloor} \in \mathcal{A}_3$, and the rest samples belonging to \mathcal{A}_4 .

Table 1 reports the average and standard error (in parentheses) of tensor decomposition error and clustering error based on 50 data replications. In terms of decomposition accuracy, it is clearly seen that our method outperforms the competitors in almost all scenarios. When the dimension d_1 increases from 20 to 40, the estimation error increases, as the decomposition becomes more challenging. When the signal μ increases from 1 to 1.2, i.e., the tensor decomposition weight w^* increases, the estimation error reduces dramatically. In terms of clustering accuracy, the clustering based on the three decomposition methods consistently outperform the one based on the vectorized data without any decomposition. Among those three, our approach performs the best, which demonstrates the usefulness of incorporation of both sparsity and fusion structures in tensor decomposition. We also note that, when $N = 100$ and $\mu = 1.2$, our structured tensor factorization yields a slightly larger estimation error than the tensor truncated power method. However, the clustering error based on our approach is about two times smaller than theirs.

5.3 Clustering of 3D tensor data

We simulate the three-dimensional tensor samples, $\mathcal{X}_i \in \mathbb{R}^{d_1 \times d_2 \times d_3}$, $i = 1, \dots, N$. We vary the sample size $N = \{50, 100\}$, the signal level $\mu = \{0.6, 0.8\}$, and set $d_1 = d_2 = d_3 = 20$. We did not consider $d_1 = 40$, since the computation is too expensive for the alternative solution that applies K -means to the vectorized data. The unnormalized components are generated as,

$$\begin{aligned} \tilde{\beta}_{11}^* = \tilde{\beta}_{21}^* = \tilde{\beta}_{31}^* &= (\underbrace{\mu, \dots, \mu}_5, \underbrace{-\mu, \dots, -\mu}_5, \underbrace{0, \dots, 0}_{10}), \quad \tilde{\beta}_{41}^* = (\underbrace{\mu, \dots, \mu}_{\lfloor N/2 \rfloor}, \underbrace{-\mu, \dots, -\mu}_{\text{the rest}}); \\ \tilde{\beta}_{12}^* = \tilde{\beta}_{22}^* = \tilde{\beta}_{32}^* &= (\underbrace{0, \dots, 0}_{10}, \underbrace{\mu, \dots, \mu}_5, \underbrace{-\mu, \dots, -\mu}_5), \quad \tilde{\beta}_{42}^* = (\underbrace{-\mu, \dots, -\mu}_{\lfloor N/4 \rfloor}, \underbrace{\mu, \dots, \mu}_{\lfloor N/2 \rfloor}, \underbrace{-\mu, \dots, -\mu}_{\text{the rest}}). \end{aligned}$$

Table 2 reports the average and standard error (in parentheses) of tensor decomposition error and clustering error based on 50 data replications. Again we observe similar qualitative patterns in 3D tensor clustering as in 2D matrix clustering, except that the advantage of our method is even more prominent. It is also noted that the clustering error of applying

Table 1: Clustering of 2D matrices. Reported are the average and standard error (in parentheses) of tensor decomposition error and clustering error based on 50 data replications. For tensor decomposition, we compare our proposed structured tensor factorization method (STF) with the tensor truncated power method (TTP) of [Sun et al. \(2016\)](#), and the generalized lasso penalized tensor decomposition method (GLTD) of [Madrid-Padilla and Scott \(2016\)](#). For clustering, we compare K -means clustering based on STF (denoted as dynamic tensor clustering, DTC), TTP, GLTD, and the vectorized data, respectively.

| $d_1 = d_2$ | N | μ | Decomposition accuracy | | | |
|---------------------|-----|-------|------------------------|----------------------|---------------|---------------|
| | | | STF | TTP | GLTD | |
| 20 | 50 | 1 | 0.584 (0.034) | 0.669 (0.033) | 0.861 (0.028) | |
| | | 1.2 | 0.210 (0.035) | 0.275 (0.035) | 0.51 (0.037) | |
| | 100 | 1 | 0.512 (0.038) | 0.566 (0.036) | 0.797 (0.033) | |
| | | 1.2 | 0.233 (0.038) | 0.218 (0.032) | 0.483 (0.046) | |
| 40 | 50 | 1 | 0.661 (0.034) | 0.788 (0.024) | 0.943 (0.018) | |
| | | 1.2 | 0.338 (0.043) | 0.502 (0.042) | 0.747 (0.044) | |
| | 100 | 1 | 0.569 (0.029) | 0.737 (0.029) | 0.927 (0.024) | |
| | | 1.2 | 0.285 (0.042) | 0.420 (0.043) | 0.688 (0.043) | |
| Clustering accuracy | | | | | | |
| $d_1 = d_2$ | N | μ | DTC | TTP | GLTD | |
| | | | | | vectorized | |
| 20 | 50 | 1 | 0.201 (0.013) | 0.319 (0.017) | 0.324 (0.021) | 0.306 (0.006) |
| | | 1.2 | 0.033 (0.008) | 0.109 (0.017) | 0.165 (0.014) | 0.255 (0.000) |
| | 100 | 1 | 0.186 (0.017) | 0.274 (0.020) | 0.326 (0.021) | 0.282 (0.002) |
| | | 1.2 | 0.046 (0.010) | 0.096 (0.015) | 0.167 (0.017) | 0.253 (0.000) |
| 40 | 50 | 1 | 0.201 (0.011) | 0.361 (0.013) | 0.297 (0.018) | 0.429 (0.007) |
| | | 1.2 | 0.079 (0.010) | 0.201 (0.012) | 0.198 (0.012) | 0.262 (0.002) |
| | 100 | 1 | 0.211 (0.010) | 0.361 (0.016) | 0.372 (0.020) | 0.374 (0.006) |
| | | 1.2 | 0.053 (0.009) | 0.170 (0.015) | 0.217 (0.014) | 0.253 (0.000) |

K -means to the vectorized data without any decomposition is at least 0.253 even when the signal strength increases. This is due to the fact that the method always mis-estimates the number of clusters K . By contrast, our method could estimate K correctly. Figure 3 illustrates the gap statistic of both methods in one data replication with $\mu = 0.6$, where the true value $K = 4$ in this example. Moreover, the tuning time for the method with the vectorized data is very long due to expensive computation of gap statistic in this ultrahigh dimensional setting. This example suggests that our method of clustering after structured tensor factorization has clear advantages in not only computation but also the tuning and the subsequent clustering accuracy compared to the simple alternative solution that directly applies clustering to the vectorized data.

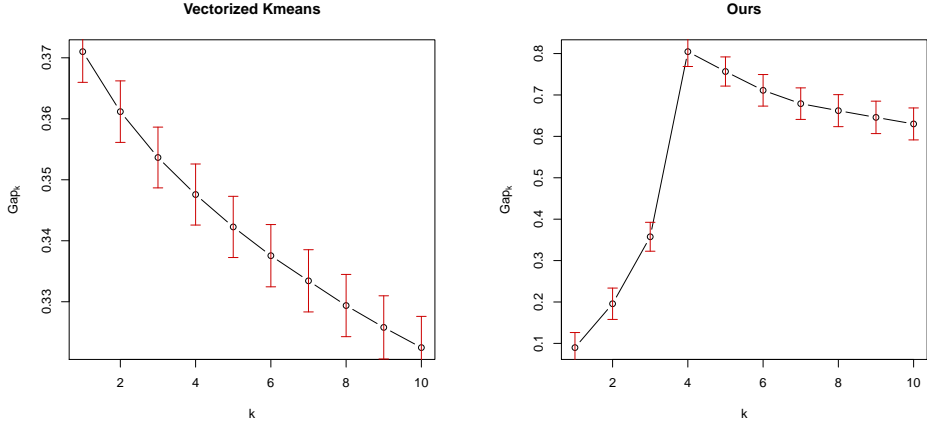
Table 2: Clustering of 3D tensors. Reported are the average and standard error (in parentheses) of tensor decomposition error and clustering error based on 50 data replications. For tensor decomposition, we compare our proposed structured tensor factorization method (STF) with the tensor truncated power method (TTP) of [Sun et al. \(2016\)](#), and the generalized lasso penalized tensor decomposition method (GLTD) of [Madrid-Padilla and Scott \(2016\)](#). For clustering, we compare K -means clustering based on STF (denoted as dynamic tensor clustering, DTC), TTP, GLTD, and the vectorized data, respectively.

| $d_1 = d_2 = d_3$ | N | μ | Decomposition accuracy | | |
|-------------------|-----|-------|------------------------|---------------|---------------|
| | | | STF | TTP | GLTD |
| 20 | 50 | 0.6 | 0.268 (0.061) | 0.835 (0.038) | 0.614 (0.063) |
| | | 0.8 | 0.012 (0.001) | 0.166 (0.052) | 0.255 (0.058) |
| | 100 | 0.6 | 0.194 (0.056) | 0.660 (0.058) | 0.422 (0.077) |
| | | 0.8 | 0.009 (0.001) | 0.306 (0.060) | 0.144 (0.053) |
| $d_1 = d_2 = d_3$ | N | μ | Clustering accuracy | | |
| | | | DTC | TTP | GLTD |
| 20 | 50 | 0.6 | 0.103 (0.028) | 0.369 (0.021) | 0.294 (0.033) |
| | | 0.8 | 0.000 (0.000) | 0.06 (0.024) | 0.099 (0.028) |
| | 100 | 0.6 | 0.076 (0.027) | 0.304 (0.027) | 0.182 (0.038) |
| | | 0.8 | 0.000 (0.000) | 0.133 (0.028) | 0.059 (0.024) |
| | | | | | vectorized |

6 Real data analysis

We illustrate our dynamic tensor clustering method through a brain dynamic connectivity analysis based on resting-state functional magnetic resonance imaging (fMRI). Meanwhile we emphasize that our proposed method can be equally applied to many other dynamic tensor applications as well. The data is from the Autism Brain Imaging Data Exchange (ABIDE), a study of autism spectrum disorder (ASD) ([Di Martino et al., 2014](#)). ASD is an increasingly prevalent neurodevelopmental disorder, characterized by symptoms such as social difficulties, communication deficits, stereotyped behaviors and cognitive delays ([Rudie et al., 2013](#)). The data were obtained from multiple imaging sites. We have chosen to focus on the fMRI data from the USM site only, due to its relatively large sample size; meanwhile the sample size is not too large so to ensure the computation of applying K -means clustering to the vectorized data is feasible. See more discussion on the computation aspect in our first task and Table 3. The data consists of resting-state fMRI of 57 subjects, of whom 22 have ASD, and 35 are normal controls. The fMRI data has been preprocessed, and is summarized as a 116×146 spatial-temporal matrix for each subject, corresponding to the time course with length 146 of 116 parcellated brain regions-of-interest (ROI) from the Anatomical Automatic Labeling

Figure 3: Gap statistics of clustering 3D tensor samples based on a single data replication. Left panel shows the gap statistic from applying K -means to the vectorized tensor data, and the right panel shows that after structured tensor factorization. The true number of clusters is 4 in this example.



(AAL) atlas. We consider two specific tasks in our analysis that investigate brain dynamic connectivity patterns using the sliding window approach. The corresponding dynamic tensor, by construction, has its sub-tensors along the time mode highly correlated, due to the fact that the sliding windows are overlapping with each other. In the first task, we aim to cluster the subjects based on their dynamic brain functional architectures. In the second task, we aim to uncover the dynamic behavior of the brain connectivity of each diagnostic group and compare between the ASD subjects with the normal control.

Specifically, in the first task, the targeting tensor $\mathcal{T} \in \mathbb{R}^{116 \times 116 \times t \times n}$, which stacks a sequence of correlation matrices of dimension 116×116 corresponding to 116 brain regions over t sliding time windows, and n is the total number of subjects and equals 57 in this example. There are two parameters affecting the moving windows, the width of the window and the step size of each movement. We combined these two into a single parameter, the number of moving windows t , by fixing the width of moving window at 20. We varied the value of t among $\{1, 30, 50, 80\}$ to examine its effect on the subsequent clustering performance. When $t = 1$, it reduces to the usual static connectivity analysis. Our goal is to cluster along the last mode of \mathcal{T} , i.e., the mode of individual subjects, based on their dynamic functional connectivity patterns. We fixed the fusion parameter at 0.9, and did not impose any sparsity constraint, since our focus in the first task is on the overall dynamic connectivity behavior rather than individual connections. We fixed the number of clusters at $K = 2$,

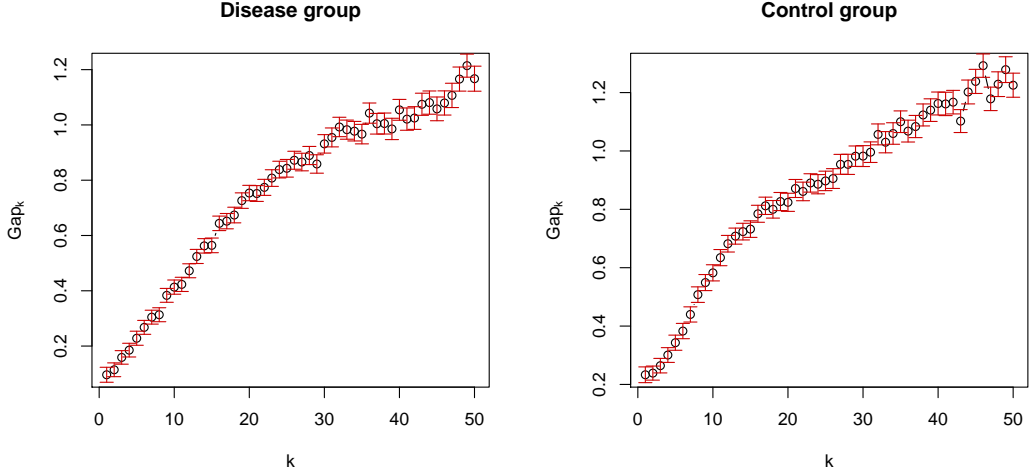
Table 3: Clustering of the ABIDE data along the *subject mode*. Reported is the clustering accuracy for our dynamic tensor clustering method (DTC), and K -means clustering applied to the vectorized data (K -means), with different numbers of sliding windows.

| Number of sliding windows | DTC | K -means |
|---------------------------|----------------------|--------------------|
| 1 | $26/57 = 0.456$ | $27/57 = 0.474$ |
| 30 | $22/57 = 0.386$ | $27/57 = 0.474$ |
| 50 | $18/57 = 0.316$ | $28/57 = 0.491$ |
| 80 | 15/57 = 0.263 | NA (out of memory) |

and compared our estimated clusters with the subject’s disease status, which is treated as the true cluster membership in this analysis. Moreover, we compared our method with the K -means clustering applied to the vectorized tensor samples, a solution commonly used in brain dynamic functional connectivity analysis (Allen et al., 2014). We report the clustering accuracy in Table 3. We make a few observations. First, the clustering accuracy based on dynamic connectivity ($t > 1$) is consistently better than the one based on static connectivity ($t = 1$). This suggests that the underlying connectivity pattern is likely dynamic rather than static for this data. Second, the clustering accuracy of our method is considerably better than that of applying K -means to the vectorized data. Moreover, our method is computationally much more efficient. Actually the method that directly applies K -means to the vectorized data ran out of memory in the case when $t = 80$, as it involves computation of a vector of dimension over 10^6 , and the standard implementation of K -means in R that we used attempted to save a gigantic $116 \times 116 \times 80^2$ tensor. Although this implementation can be surely optimized to account for the ultrahigh dimensionality of tensor data, it is not the focus of this article. Third, the number of moving windows does indeed affect the clustering accuracy, as one would naturally expect. In practice, we recommend experimenting with multiple values of t . Furthermore, we can treat t as another tuning parameter.

In the second task, we aim to compare the dynamic connectivity patterns between the ASD group and the normal control. Toward that end, the targeting tensor $\mathcal{T} \in \mathbb{R}^{116 \times 116 \times n_g \times t}$, where n_g denotes the number of subjects in each diagnostic group; in our example, $n_1 = 22$ and $n_0 = 35$. In light of the results from task 1, we fixed the number of moving time windows at $t = 80$. Our goal is to cluster along the last mode of \mathcal{T} , i.e., the time mode, to examine the dynamic behavior, if any, of the functional connectivity networks. We carried out two clustering analysis, one for each diagnostic group. We employed the BIC criterion discussed in Section 3.3 to select the rank, the sparsity parameter, and the fusion parameter, and then

Figure 4: Clustering of the ABIDE data along the *time mode*. The gap statistic as a function of the number of clusters for the ASD group and the control group. It chose $K = 7$ for the ASD group, and $K = 12$ for the control group.



tuned the number of clusters K using the gap statistic. For both the ASD and the normal control group, the selected rank is 5. The selected sparsity parameter is 0.9, and the fusion parameter is 0.5, suggesting that in the estimated decomposition components, there are 10% zero entries, and about 40 unique values along the time mode. Figure 4 further shows the gap statistic as a function of the number of clusters for both diagnostic groups. Accordingly, it selects $K = 7$ for the ASD group, and $K = 12$ for the normal control. Moreover, we have observed that, for the ASD group, the clustering membership changed 10 times along the sliding windows, whereas it changed 14 times for the control. This on one hand suggests that both groups of subjects exhibit dynamic connectivity changes over time. More importantly, the change of the state of connectivity is less frequent for the ASD group than the control. This finding agrees with the literature in that the ASD subjects are usually found less active in brain connectivity patterns (Solomon et al., 2009; Gotts et al., 2012; Rudie et al., 2013).

Appendix

The appendix contains the technical details of theorems and is available upon request.

References

ALLEN, E. A., DAMARAJU, E., PLIS, S. M., ERHARDT, E. B., EICHELE, T. and CALHOUN, V. D. (2014). Tracking whole-brain connectivity dynamics in the resting state. *Cerebral Cortex* **24** 663.

ANANDKUMAR, A., GE, R. and JANZAMIN, M. (2014). Guaranteed non-orthogonal tensor decomposition via alternating rank-1 updates. *arXiv preprint arXiv:1402.5180* .

ASTON, J. and KIRCH, C. (2012). Estimation of the distribution of change-points with application to fmri data. *Annals of Applied Statistics* **6** 1906–1948.

BRUCE, N., MURTHI, B. and RAO, R. C. (2016). A dynamic model for digital advertising: The effects of creative format, message content, and targeting on engagement. *Journal of Marketing Research* To Appear.

CAO, X., WEI, X., HAN, Y., YANG, Y. and LIN, D. (2013). Robust tensor clustering with non-greedy maximization. In *Proceedings of the Twenty-Third International Joint Conference on Artificial Intelligence*.

CHI, E. C. and ALLEN, G. I. (2017). Convex biclustering. *Biometrics* **73** 10–19.

CHI, E. C. and LANGE, K. (2015). Splitting methods for convex clustering. *Journal of Computational and Graphical Statistics* 994–1013.

DI MARTINO, A., YAN, C.-G., LI, Q., DENIO, E., CASTELLANOS, F. X., ALAERTS, K., ANDERSON, J. S., ASSAF, M., BOOKHEIMER, S. Y., DAPRETTO, M., DEEN, B., DELMONTE, S., DINSTEIN, I., ERTL-WAGNER, B., FAIR, D. A., GALLAGHER, L., KENNEDY, D. P., KEOWN, C. L., KEYSERS, C., LAINHART, J. E., LORD, C., LUNA, B., MENON, V., MINSHEW, N. J., MONK, C. S., MUELLER, S., MULLER, R.-A., NEBEL, M. B., NIGG, J. T., O'HEARN, K., PELPHREY, K. A., PELTIER, S. J., RUDIE, J. D., SUNAERT, S., THIOUX, M., TYSZKA, J. M., UDDIN, L. Q., VERHOEVEN, J. S., WENDEROTH, N., WIGGINS, J. L., MOSTOFSKY, S. H. and MILHAM, M. P. (2014). The autism brain imaging data exchange: Towards a large-scale evaluation of the intrinsic brain architecture in autism. *Molecular Psychiatry* **19** 659–667.

DING, S. and COOK, R. D. (2015). Tensor sliced inverse regression. *Journal of Multivariate Analysis* **133** 216–231.

FORNITO, A., ZALESKY, A. and BREAKSPEAR, M. (2013). Graph analysis of the human connectome: Promise, progress, and pitfalls. *NeuroImage* **80** 426–444.

GOTTS, S., SIMMONS, W., MILBURY, L., WALLACE, G., COX, R. and MARTIN, A. (2012). Fractionation of social brain circuits in autism spectrum disorders. *Brain* 2711–2725.

HOCKING, T., VERT, J.-P., BACH, F. and JOULIN, A. (2011). Clusterpath: An algorithm for clustering using convex fusion penalties. *Proceedings of the Twenty Eighth International Conference on Machine Learning* .

HUANG, J., SHEN, H. and BUJA, A. (2009). The analysis of two-way functional data using two-way regularized singular value decompositions. *Journal of the American Statistical Association* **104** 1609–1620.

HUTCHISON, R. M., WOMELSDORF, T., ALLEN, E. A., BANDETTINI, P. A., CALHOUN, V. D., CORBETTA, M., PENNA, S. D., DUYN, J. H., GLOVER, G. H., GONZALEZ-CASTILLO, J., HANDWERKER, D. A., KEILHOLZ, S., KIVINIEMI, V., LEOPOLD, D. A., DE PASQUALE, F., SPORNS, O., WALTER, M. and CHANG, C. (2013). Dynamic functional connectivity: Promise, issues, and interpretations. *NeuroImage* **80** 10.1016/j.neuroimage.2013.05.079.

JI, S., ZHANG, W. and LIU, J. (2012). A sparsity-inducing formulation for evolutionary co-clustering. *International conference on knowledge discovery and data mining* .

KOLDA, T. and BADER, B. (2009). Tensor decompositions and applications. *SIAM Review* **51** 455–500.

LEE, M., SHEN, H., HUANG, J. Z. and MARRON, J. S. (2010). Biclustering via sparse singular value decomposition. *Biometrics* **66** 1087–1095.

LENG, C. and TANG, C. Y. (2012). Sparse matrix graphical models. *Journal of the American Statistical Association* 1187–1200.

LI, R., ZHANG, W., ZHAO, Y., ZHU, Z. and JI, S. (2015). Sparsity learning formulations for mining time-varying data. *IEEE Transactions on Knowledge and Data Engineering* **27** 1411–1423.

LIU, J., MUSIALSKI, P., WONKA, P. and YE, J. (2013). Tensor completion for estimating missing values in visual data. *IEEE Transactions on Pattern Analysis and Machine Intelligence* **35** 208–220.

LIU, T., YUAN, M. and ZHAO, H. (2017). Characterizing spatiotemporal transcriptome of human brain via low rank tensor decomposition. *arXiv preprint arXiv:1702.07449* .

MA, P. and ZHONG, W. (2008). Penalized clustering of large scale functional data with multiple covariates. *Journal of the American Statistical Association* **103** 625–636.

MADRID-PADILLA, O.-H. and SCOTT, J. G. (2016). Tensor decomposition with generalized lasso penalties. *arXiv* .

ROMERA-PAREDES, B. and PONTIL, M. (2013). A new convex relaxation for tensor completion. In *Advances in Neural Information Processing Systems*.

RUDIE, J., BROWN, J., BECK-PANCER, D., HERNANDEZ, L., DENNIS, E., THOMPSON, P., BOOKHEIMER, S. and DAPRETTO, M. (2013). Altered functional and structural brain network organization in autism. *NeuroImage : Clinical* **2** 79–94.

SEIGAL, A., BEGUERISSE-DIAZ, M., SCHOEBERL, B., NIEPEL, M. and HARRINGTON, H. A. (2016). Tensors and algebra give interpretable groups for crosstalk mechanisms in breast cancer. *arXiv preprint arXiv:1612.08116* .

SHEN, X., HUANG, H. and PAN, W. (2012a). Simultaneous supervised clustering and feature selection over a graph. *Biometrika* **99** 899–914.

SHEN, X., PAN, W. and ZHU, Y. (2012b). Likelihood-based selection and sharp parameter estimation. *Journal of the American Statistical Association* **107** 223–232.

SOLOMON, M., OZONOFF, S., URSU, S., RAVIZZA, S., CUMMINGS, N., LY, S. and CARTER, C. (2009). The neural substrates of cognitive control deficits in autism spectrum disorders. *Neuropsychologia* **47** 2515–2526.

SUN, W., LU, J., LIU, H. and CHENG, G. (2016). Provable sparse tensor decomposition. *Journal of the Royal Statistical Society, Series B* To Appear.

TIBSHIRANI, R., SAUNDERS, M., ROSSET, S., ZHU, J. and KNIGHT, K. (2005). Sparsity and smoothness via the fused lasso. *Journal of the Royal Statistical Society: Series B* **67** 91–108.

TIBSHIRANI, R., WALTHER, G. and HASTIE, T. (2001). Estimating the number of clusters in a dataset via the gap statistic. *Journal of the Royal Statistical Society: Series B* **63** 411–423.

TIBSHIRANI, R. J. and TAYLOR, J. (2011). The solution path of the generalized lasso. *Annals of Statistics* **39** 1335–1371.

WANG, J. (2010). Consistent selection of the number of clusters via cross validation. *Biometrika* **97** 893–904.

WANG, J. (2015). Joint estimation of sparse multivariate regression and conditional graphical models. *Statistica Sinica* **25** 831–851.

WANG, J. and FANG, Y. (2013). Analysis of presence-only data via semisupervised learning approaches. *Computational Statistics and Data Analysis* **59** 134–143.

WANG, Y., XU, H. and LENG, C. (2013). Provable subspace clustering: When lrr meets ssc. *Advances in Neural Information Processing Systems* .

WU, T., BENSON, A. R. and GLEICH, D. F. (2016). General tensor spectral co-clustering for higher-order data. *Advances in Neural Information Processing Systems* .

XU, P., ZHANG, T. and GU, Q. (2017). Efficient algorithm for sparse tensor-variate gaussian graphical models via gradient descent. *Proceedings of the 20th International Conference on Artificial Intelligence and Statistics (AISTATS)* .

YUAN, M. and KENDZIORSKI, C. (2006). A unified approach for simultaneous gene clustering and differential expression identification. *Biometrics* **62** 1089–1098.

YUAN, M. and ZHANG, C. (2016a). Incoherent tensor norms and their applications in higher order tensor completion. *arXiv* .

YUAN, M. and ZHANG, C. (2016b). On tensor completion via nuclear norm minimization. *Foundations of Computational Mathematics* **16** 1031–1068.

ZHANG, A. (2016). Cross: Efficient low-rank tensor completion. *arXiv* .

ZHOU, H., LI, L. and ZHU, H. (2013). Tensor regression with applications in neuroimaging data analysis. *Journal of the American Statistical Association* **108** 540–552.

ZHU, H., ZHANG, H., IBRAHIM, J. and PETERSON, B. (2007). Statistical analysis of diffusion tensors in diffusion-weighted magnetic resonance image data. *Journal of the American Statistical Association* **102** 1081–1110.

ZHU, Y. (2017). An augmented admm algorithm with application to the generalized lasso problem. *Journal of Computational and Graphical Statistics* **26** 195–204.

ZHU, Y., SHEN, X. and PAN, W. (2014). Structural pursuit over multiple undirected graphs. *Journal of the American Statistical Association* **109** 1683–1696.